Proceedings of the 17th International Heat Transfer Conference, IHTC-17
14 – 18 August 2023, Cape Town, South Africa

IHTC-17 | ID: 0572

VAPOUR BUBBLE FORMATION IN SUBCOOLED FLOW BOILING THROUGH A VERTICAL CHANNEL

Zengchao Chen[1], Surya Narayan[1], Aleksei S. Lobasov[1,2], Konstantin S. Pervunin[1], Christos N. Markides[1,2,*]

[1]Clean Energy Processes (CEP) Laboratory, Department of Chemical Engineering, Imperial College London, London SW7 2AZ, United Kingdom
[2]Kutateladze Institute of Thermophysics, Siberian Branch of the Russian Academy of Sciences, Novosibirsk 630090, Russia

N.B.: This is the ACCEPTED MANUSCRIPT version of this article. The final, published version of the article can be found at: https://doi.org/10.1615/IHTC17.150-110

ABSTRACT

Flow boiling in miniaturised channels is one of the most promising solutions for the efficient heat removal from next-generation high-power-density electronic devices. The existing models in design tools used to predict boiling heat transfer rates are largely based on empirical correlations and are very specific for the regime of boiling observed. A unified model that would be entirely based on the underlying physics of boiling and vapour bubble formation is an elusive task primarily due to our limited understanding of flow boiling. In this paper, we present results from an experimental investigation of the fundamental physics of a single vapour bubble formation inside a vertically oriented minichannel with a square cross-section and a hydraulic diameter of 5 mm. The experiments were performed for a selected set of mass fluxes (33–100 kg/m^{2}s) and inlet subcooling degrees (5–15 K) using HFE-7100 as the working fluid. The test section is optically accessible from all directions, with one side of the channel fitted with an indium tin oxide (ITO) coated sapphire substrate to locally heat the fluid and generate vapour bubbles. Using diffuse backlight and a high-speed camera, visual observations of the vapour bubble formation process from a natural nucleation site for heat fluxes in the range 1.8-2.2 kW/m^2 was conducted. The recorded time-lapse images were post-processed to extract the dynamic variations of vapour bubble features including width, height, base diameter, equivalent diameter, growth rate and sliding velocity over multiple bubble cycles. Using the least square circle fit method, the dynamic variations of upstream and downstream contact angles were also quantified. The temporal evolution of the bubble dynamic characteristics was compared to the isothermal bubble growth model in order to assess the conformity of their results, and gain insight into changes in the superheat level of the liquid phase adjacent to the growing vapour bubble.

KEY WORDS: Miniaturised channel, Subcooled boiling flow, Vapour bubble dynamics, Visualisation.

1. INTRODUCTION

The ability to transport a significant amount of thermal energy across a minimum temperature difference between a heated surface and a working fluid has made boiling flows a potent alternative to conventional single-phase cooling techniques. In order to achieve the cooling requirements of the electronics industry, miniaturised channels that utilise the phase change process have recently attracted the attention of the scientific and engineering community [1]. Even though significant strides have been made in recent years through rigorous experimental research [2] and numerical modelling [3], challenges associated with the multiscale physics and transient phenomena of boiling flows persist.

*Corresponding author: c.markides@imperial.ac.uk

The initial formation of a vapour bubble in a subcooled boiling flow is a highly localized phenomenon, so conventional measurements of bulk flow parameters (primarily pressure and temperature) at the inlet and outlet of a test section provides only limited understanding of the interaction of hydrodynamics and thermal processes that take place where boiling occurs. Apart from few recent experimental efforts to directly study the fundamental physics of the inception and growth of a single vapour bubble in a flow through a minichannel, and to quantify its departure characteristics based on the properties of an isolated nucleation site [4, 5], experimental research in this direction is mainly limited to the classification of the observed flow regimes depending on the distribution of the continuous and dispersed phases [6]: slug, churn and annular. It is also worth noting that in many studies, e.g., Refs. [4, 5], water is used as the coolant, and since water is an ionic liquid with a relatively high saturation temperature (T_{sat} = 373.1 K) at atmospheric pressure (P_s = 101.3 kPa), its applicability to cooling electronic components is limited in practice.

For this reason, dielectric electronic cooling liquids, such as 3M HydroFluoroEther-7100 (HFE-7100), with lower saturation temperatures (e.g., T_{sat} = 334.3 K at P_s = 101.3 kPa for HFE-7100) have been purposefully developed for use in electronics cooling applications. However, these fluids also have a lower surface tension to promote wetting of the heated surface in comparison with deionised water (Table 1). It is well established in the literature that low values of the surface tension of the working fluid can lead to a decrease in the timescale of bubble growth and facilitate the early departure of a vapour bubble from a nucleation site. Since a vapour bubble only interacts with the nucleation site for a brief period when an electronic fluid is employed, changes in the temperature of the surface and of the fluid adjacent to the vapour bubble can be significantly reduced relative to the case of water. In this content, the classical model of bubble growth [7] combined with experimental observations of single vapour bubble evolution can be used to promote our understanding of these phenomena, but also to indicate the measurement requirements from advanced non-invasive temperature measurement techniques [8] that we are planning to apply to these flows in future experiments.

Furthermore, the validation of interface-capturing numerical models that can be used to study internal boiling flows largely relies on the shapes of vapour bubbles obtained a decade ago [9]. As the data from Ref. [9] are for water, the characteristic time scale of bubble growth should be substantially longer compared to HFE-7100 and, consequently, numerical calculations would require significant computational resources. A reduced time scale for the vapour bubble growth process in electronic cooling fluids and refrigerants should make it possible to decrease the computational costs and, therefore, could become beneficial to the numerical modelling community.

This paper reports on an experimental investigation of the process of a vapour bubble growth in a boiling flow of HFE-7100 fluid through a vertically oriented square channel. Vapour bubbles were recorded optically using highspeed videography (HSV) and the data were post-processed to extract time variations of the bubble shape characteristics including width, height, base diameter, equivalent diameter, upstream/downstream dynamic contact angle, growth rate and sliding velocity over multiple single vapour bubble ebullition cycles from a naturally occurring nucleation site. Of interest is also the comparison of the temporal evolution of the bubble parameters to the isothermal bubble growth model, in order to assess conformity and to gain insight into changes in the superheat level of the liquid phase around growing vapour bubbles. Finally, the results were used to identify key requirements for state-of-the-art spatiotemporally resolved laser/infrared-based measurement techniques including two-colour Laser-Induced Fluorescence (2cLIF), particle image velocimetry (PIV) and infrared thermography (IRT) which are to be applied to study the single vapour bubble formation process in subcooled flow boiling.

Table 1 Physical properties of water and HFE-7100 at 25 °C and 1 bar.

Property	Water	HFE-7100
Boiling point (°C)	100	61
Density (kg/m^3)	997 (liquid); 0.8 (vapour)	1510 (liquid); 11 (vapour)
Viscosity (cP)	0.89	0.58
Surface tension (mN/m)	72	13.6

2. EXPERIMENTAL APPARATUS AND PROCEDURE

The experimental apparatus was specifically developed to reproduce various flow-boiling conditions in a minichannel and is shown schematically in Fig. 1. The test facility has a closed loop and is composed of a storage tank, peristaltic pump with a coarse inline particle filter, high-accuracy mass-flow controller, test section, condenser, two preheaters, and a bypass circuit where a pressure controller is installed. The working fluid is HFE-7100 which is kept in the storage tank equipped with a thermometer and a pressure gauge. The inline particle filter is incorporated into the pipeline immediately after the storage tank to prevent impurities exceeding 90 μm in size from entering the main flow loop. The pump capable of handling with liquids containing tracer particles drives the working fluid around the apparatus at relatively low flow rates. The mass-flow controller allows regulating and maintaining the mass flow rate through the hydraulic system at a preset level. The pressure controller in the bypass loop is required to stabilise the inlet pressure of the mass-flow controller, which is achieved by diverting a portion of the total flow rate back to the pump inlet through a connection upstream of the filter (Fig. 1). This makes it possible to substantially mitigate pulsations of the mass flow rate in the main flow circuit. To reach a desired subcooled bulk condition, two pre-heaters are utilised. Preheater-1 is a plate heat exchanger which is coupled with a circulating thermal bath filled with ethylene glycol that warms up the working fluid from ambient to a relatively high temperature. Preheater-2 is of electrical type and is connected to an AC power supply which further heats the fluid to a certain subcooling degree at the inlet of the test section (Fig. 1).

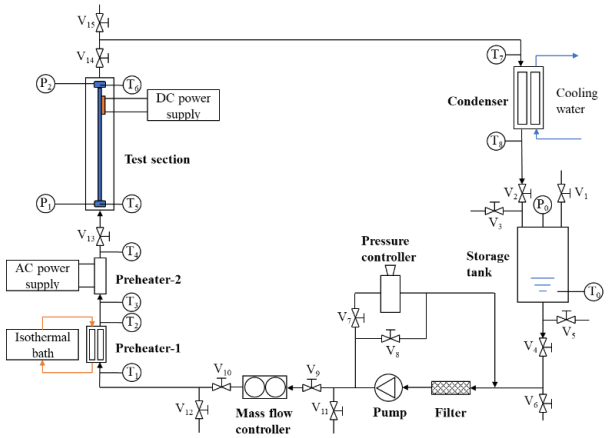


Fig. 1 Layout of the experimental apparatus to study flow boiling in a minichannel.

The working fluid then enters the test section. To initiate formation of vapour bubbles, an additional heat flux provided by Joule heating of an optically transparent ITO coating deposited on a sapphire-glass substrate and connected to a DC power supply is imposed to one of the walls of the test channel. The condenser, which is a plate heat exchanger, circulates cold tap water to cool down the working fluid exiting the test section to ambient temperature. A few sensors are connected to the facility loop to monitor its operation in real time. These include six 3-mm diameter 4-wire PT100 resistance temperature detectors (RTDs) which are placed at the inlets and outlets of the condenser and two preheaters as well as two 0.5-mm diameter sheathed T-type thermocouples along with two pressure transducers attached to the inlet and outlet of the test section. All data read by these sensors were recorded by the Keysight DAQ973A data acquisition system at a rate of 1 datapoint per second. Several valves are mounted at certain locations of the hydraulic system for the facility filling, the fluid draining and degassing, as well as the components replacement, especially the test section.

The main elements of the test section are the cover, base and pedestal that are all made of polycarbonate and vapour-polished to be optically accessible (Fig. 2a). A square groove with a cross-section of 5×5 mm was machined on the base to form a miniaturised channel with a hydraulic diameter of $D_h = 4A_c/P = 5$ mm, where A_c is the cross-sectional area of the flow and P is the wetted perimeter of the cross-section. The inlet and outlet of the test section are located at the two ends of the channel, where the

thermocouples and pressure transducers are attached to (Fig. 2b). A thin heater comprised of a 0.5-mm thick sapphire-glass substrate of dimensions of 80×10 mm coated with a thin conductive indium tin oxide (ITO) film using the vapour deposition method and supported by the pedestal is flush embedded into the channel wall (Fig. 2a). The heater is transparent to visible light to enable access of laser light into the channel for optical diagnostics of the boiling flow, while the ITO film is opaque in the infrared spectrum, thus allowing thermographic imaging of the wall temperature. The hollow pedestal makes it possible to directly record the infrared radiation emitted from the ITO coating using a high-speed infrared camera. All these components are connected with M4 bolts, with three O-rings used to seal the assembly. An entrance length of 500 mm upstream of the heater is designed to guarantee hydrodynamically fully developed flow, which is followed by an effective heated length of 60 mm and an exit length of 50 mm. Boundary conditions of the boiling flow in the test channel can be assumed to be one-side heated with a uniform heat flux, with the other three sides being adiabatic.

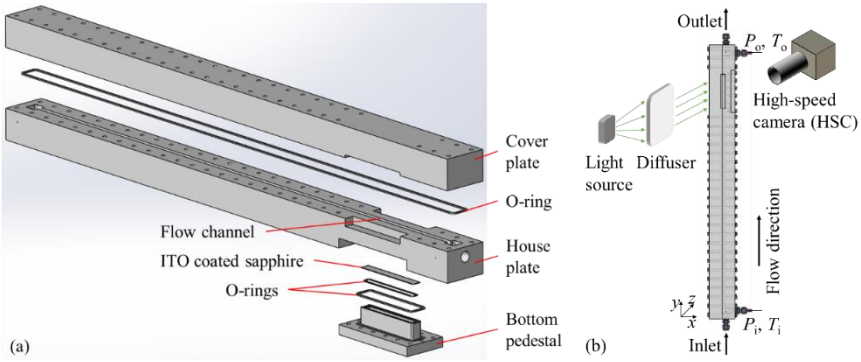


Fig. 2 Schematic of: (a) the assembly of the test section, and (b) arrangement of the visualisation system relative to the minichannel orientation.

HFE-7100 was employed as the working fluid. The experiments were performed at nearly atmospheric pressure conditions for a range of mass fluxes from 33 to 100 kg/m^2·s and inlet subcooling temperatures varied between 5 to 15 K, with the heat flux supplied to the test substrate maintained at 1.8 to 2.2 kW/m^2. Before the experiment, the fluid in the system was fully degassed through intense boiling in Preheater-2 for roughly an hour and release of the air by repeated opening of the degassing port of the storage tank. The bypass loop was initially used to establish a stable pressure, then the main circuit was activated. The mass flow rate was set to a required value by regulating the mass flow controller. After starting the cooling water circulation in the condenser, Preheater-1 was switched on to warm the fluid to an elevated temperature. Preheater-2 was further utilised to reach a certain inlet temperature. The pressure in the channel was maintained constant and equal to ambient pressure by opening the needle valve downstream of the outlet of the test section (Fig. 1). Finally, the heat flux through the heating element in the test section was adjusted in steps to achieve a desired subcooling condition of the flow boiling by changing the DC power supply. Each test run lasted for about 10 min until a thermal equilibrium state was reached, after which recordings of instrument readings, including temperature, pressure, voltage and current mass flow rate gathered by the data acquisition system, and visual data were taken. After completing measurements for the entire range of heat flux conditions, Preheater-2 was reset to vary the inlet subcooling condition. The mass flow rate was changed the last.

The arrangement of the optical system for high-speed visualisation of the boiling flow is schematically shown in Fig. 2b. In this study, the test channel was vertically oriented, with the flow directed upward. A high-power light emitting diode (LED) array was installed at one side of the test section to illuminate the heated wall of the channel. A frosted glass diffusing screen was placed between them to produce a uniformly-lit background. A Phantom VEO 310L high-speed camera (maximum resolution = 1280 × 800 at a recording rate of 3200 fps; pixel pitch = 20 μm) with a Navitar 12× tube lens fitted with a 2× zoom adaptor and 0.5× lens attachment (working distance = 165 mm) was placed at the opposite side of the test section to implement backlight visualisation. In the experiments, vapour bubble evolution

in the subcooled flow boiling conditions was recorded at the camera resolution of 1024×512 pixels and recording rate of 5000 fps. After the camera was appropriately aligned, the tip of a 0.5-mm diameter sheathed thermocouple was introduced into the measurement region through the outlet of the test section to be used as a target for accurate spatial scaling of the camera images. Visual data on the bubble growth process from an isolated natural nucleation site were post-processed using an in-house developed MATLAB code to extract the time-variations of the parameters of vapour bubbles, including their width, height, base and equivalent diameters, upstream/downstream dynamic contact angle, growth rate and sliding velocity, over multiple single bubble ebullition cycles.

3. DATA REDUCTION METHODOLOGY

Data reduction procedure is based on averaging of steady-state values read by the data acquisition system at a rate of 1 datapoint per second for a period of 20 s. The mass flux G is defined as:

$$G = \frac{\dot{m}}{W_c H_c}, \tag{1}$$

where $\dot{m}$ is the mass flow rate, W_c and H_c are the width and height of the channel. The inlet subcooling temperature ΔT_{sub} is given by:

$$\Delta T_{\mathrm{sub}} = T_{\mathrm{sat}} - T_{\mathrm{in}}, \tag{2}$$

where T_{sat} and T_{in} are the fluid saturation temperature and flow temperature at the test section inlet. The heat flux q is set as follows:

$$q = \frac{U\,I}{A_{\mathrm{h}}}, \tag{3}$$

where U and I are the voltage and current through the ITO coating and A_{h} is the surface area of the heater.

In the in-house developed MATLAB code, the contrast of raw greyscale images was first enhanced, and then the Sauvola binarisation algorithm [10] was applied to them to detect bubble boundaries. The method is a local adaptive image thresholding algorithm which dynamically calculates the intensity limit of the current pixel according to the greyscale mean and standard deviation in its neighbourhood. With this binarisation procedure, flow areas occupied by vapour bubbles were identified in the original images as shown in Fig. 3. From the binarised images (Fig. 3b), the bubble geometric parameters such as width W, height H, base diameter D_{b}, upstream and downstream dynamic contact angles θ_{u} and θ_{d} were extracted over multiple bubble growth cycles (Fig. 3c). The evaluation of the contact angles was conducted using the least square circle fit method considering the upstream or downstream half of the perimeter of a recognized bubble for θ_{u} and θ_{d}, respectively. Based on these basic parameters, the following characteristics were additionally estimated.

The bubble equivalent diameter D_{eq} is given by:

$$D_{\mathrm{eq}} = 2R_{\mathrm{eq}} = \sqrt[3]{\frac{6V_{\mathrm{eq}}}{\pi}}, \tag{4}$$

where:

$$V_{\mathrm{eq}} = \sum_{i=1}^{i=n} \frac{\pi W_i^2}{4} \Delta H \tag{5}$$

is an equivalent volume of a bubble being a superposition of disks, with diameters W_i and identical heights $\Delta H = 1$ pixel, forming the bubble contour and lying in the cross-section parallel to the wall, starting from the bubble base where $i = 1$ and finishing by its vertex where $i = n$, i.e., the overall number of the disks.

The bubble growth rate $\dot{R}$ is defined as:

$$\dot{R} = \frac{\mathrm{d}R_{\mathrm{eq}}}{\mathrm{d}t}, \tag{6}$$

The sliding velocity of a bubble along the flow direction is:

$$V_s = \frac{\mathrm{d}y_c}{\mathrm{d}t}, \tag{7}$$

where y_c is the position of the bubble geometrical centre along the y-axis.

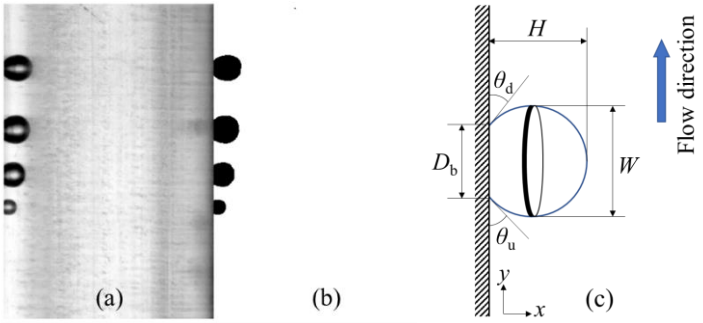


Fig. 3 (a) Raw image of a chain of vapour bubbles arisen at the wall, (b) binarised image of (a), and (c) schematic of the bubble nucleation.

4. RESULTS AND DISCUSSION

4.1 Single Bubble Features The time variations of the basic parameters of a vapour bubble shown in Fig. 4b and 4c were obtained from the image sequence in Fig. 4a by tracking the bubble originated from a nucleation site for 50 ms starting from its inception. This allows investigation of the development of the bubble attached to the wall followed by its upward motion along the heated surface. During the rapid initial growth period ($t \leq 5$ ms), the difference between the bubble width, height, base diameter and equivalent diameter is negligible and, as a result, its shape can be largely considered hemispherical. As the bubble grows ($t > 5$ ms), its width and equivalent diameter become noticeably larger than its height, with its shape changed to an oblate ellipsoid. It is widely accepted in the literature that a rapid change in the bubble shape can lead to its early detachment from the wall [12] – a topic of future research. For $t > 30$ ms, the bubble base diameter decreases rapidly, while its width, height and equivalent diameter continue to increase, indicating a probable bubble lift-off. When $t > 40$ ms, the width and equivalent diameter begin to decrease, thus giving evidence about the interaction of the bubble with the cold bulk fluid leading to vapour condensation. Furthermore, the sliding velocity of the bubble in the flow direction derived as the time derivative of its position along the *y*-axis (Fig. 4c) gradually increases as it moves away from the nucleation site. Meanwhile, its *x*-coordinate in Fig. 4c exhibits a time behaviour similar to the bubble height curve in Fig. 4b and looks relatively invariant over a short time period, thus suggesting that the bubble motion along the *x*-axis is insignificant.

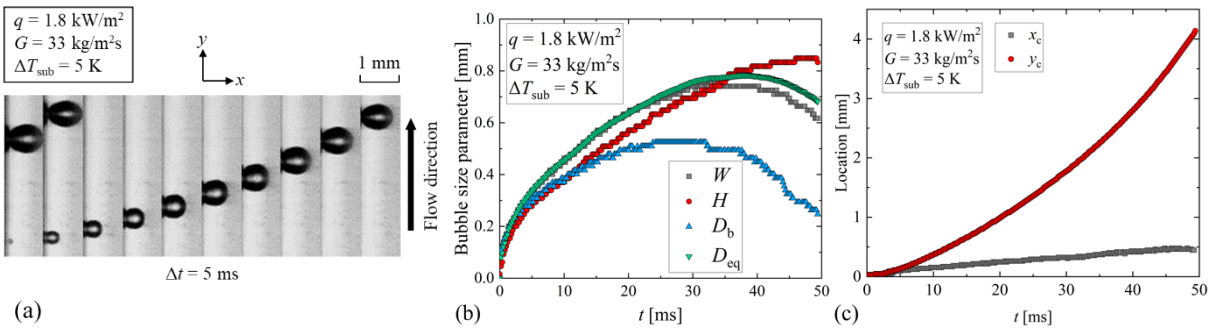


Fig. 4 (a) Time-lapse images of vapour bubble evolution, (b) evolution of the main geometrical parameters of the same bubble during a single cycle of its growth, and (c) changes in the bubble centre location over the same period. Test conditions: q = 1.8 kW/m^2, G = 33 kg/m^{2}s and ΔT_{sub} = 5 K.

In the subcooled flow boiling regime, both upstream and downstream dynamic contact angles that the bubble makes with the heated surface equal approximately 70° at the time instances where the bubble is nearly hemispherical (Fig. 5a). As it grows, both angles decrease gradually to zero. This trend accords well with the theoretical prediction by Ardron et al. [13] in the case of pool boiling using an equilibrium thermodynamic model. It is also worth noting that the magnitudes of θ_u and θ_d are slightly different,

which can be explained by the buoyancy and inertia forces that push the bubble downstream, resulting in the asymmetry of its shape due to the friction against the wall. Further efforts on improving the accuracy of the contact angle measurement using an advanced laser-induced fluorescence technique will be made to accurately segment the bubble interface.

Hereinafter, the data reduction methodology is only used for $t \leq 30$ ms, which matches the period where the bubble grows and slides without lifting-off or condensing. In order to reduce the overall level of noise and the amplitude of data fluctuations, both parameters $\dot{R}$ and V_s, being respectively the time derivative of the bubble size and position (Fig. 4b and 4c), were obtained at equal time intervals of 1.6 to 2.4 ms depending on the data quality as shown in Fig. 5b and 5c. Immediately after its inception ($t = 0$ ms), the vapour bubble expands very quickly but, as it enlarges, its growth rate is substantially reduced, becoming four times less from $\dot{R} = 0.04$ m/s at $t = 2$ ms to $\dot{R} = 0.01$ m/s after the lapse of 10 ms from the start of the bubble ebullition cycle. Then $\dot{R}$ gradually slides down to 0.005 m/s at $t = 30$ ms (Fig. 5b). This trend is in line with the classical model by Mikic et al. [7] based on the theoretical framework that the growth process is completely controlled by diffusion of thermal energy across the bubble interface from superheated liquid surrounding it. At the initial moment of time, the temperature of the superheated liquid is higher than that inside the bubble and, therefore, the liquid evaporates much faster than the vapour condensation, leading to a rapid increase of the bubble size (Fig. 5b). As the bubble expands, the superheated liquid is chilled due to the evaporative cooling effect and, as a result, the bubble growth begins to wind down (Fig. 5b). The bubble sliding velocity regarded as a vertical displacement of its geometrical centre position for a time interval is found to increase with time, but the bubble acceleration decreases at the same time (Fig. 5c). The fundamental cause of this behaviour is still unknown and requires further investigation.

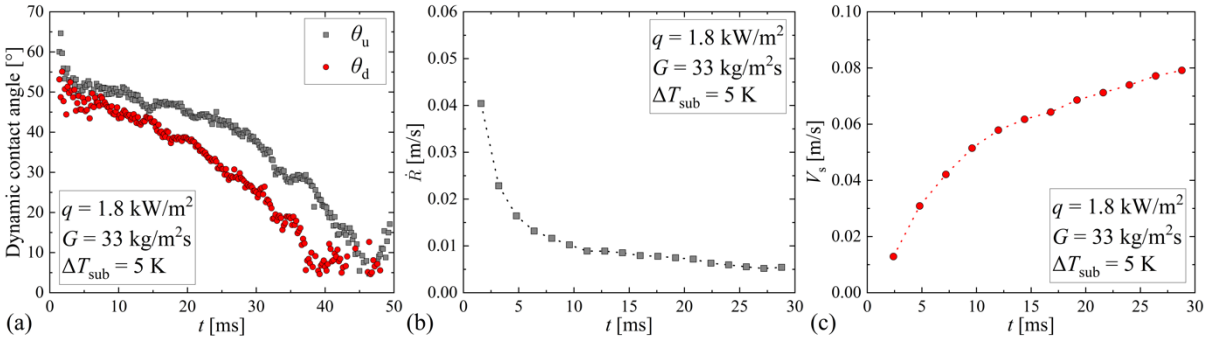


Fig. 5 Time variations of the: (a) upstream and downstream dynamic contact angles, (b) bubble growth rate, and (c) bubble sliding velocity.

Next, we compare the bubble size dynamics derived from the experimental data and using the isothermal model by Mikic et al. [7] to evaluate their goodness and gain insights into the evaporative cooling effect. As the bubble interacts with the nucleation site only for a short period at the initial stage of evolution, a change in the temperature of the wall and/or the surrounding superheated fluid could be significantly small for refrigerants like HFE-7100 due to their relatively low latent heat of vaporisation in comparison with water [4, 5]. It is seen in Fig. 6 that the experimental curve of the bubble growth coincides satisfactorily (RMS error ≈ 0.02 mm) with the theoretical relationship generated for a superheat level of $\Delta T_{\mathrm{sup}} = T_{\mathrm{sl}} - T_{\mathrm{sat}} = 0.1$ K, where T_{sl} is the temperature of the superheated liquid around the bubble. This means that, during the bubble growth, the temperature fluctuations of an order of ~ 0.1 K with respect to the saturation liquid temperature are expected to occur in the superheated liquid around the bubble. To verify this, the sensitivity of an experimental technique used must be sufficient to resolve a temperature difference of nearly $\Delta T = \Delta T_{\mathrm{sub}} + \Delta T_{\mathrm{sup}} = 5.1$ K. It is important to note that the theoretical model assumes that the physical properties of the working liquid correspond to the bulk conditions.

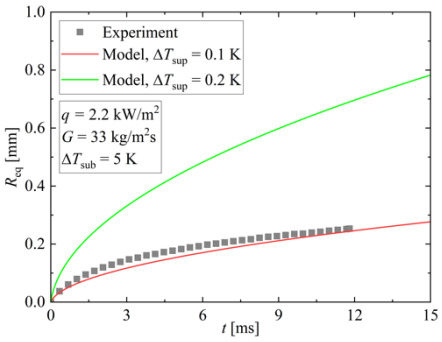


Fig. 6 Comparison of time variations of the bubble radii determined experimentally and calculated by the isothermal model by Mikic et al. [7] for two superheat levels ΔT_{sup}. Test condition: q = 2.2 kW/m^2, G = 33 kg/m^{2}s and ΔT_{sub} = 5 K.

4.2 Flow Conditions An increase in the imposed heat flux q results in a significant difference in the bubble growth rate right after the vapour bubble inception (Fig. 7a). However, after the initial (rapid) stage of evolution, the two curves almost collapse with each other when $t = 3$ ms. It is vastly unknown how a change in the initial rate of growth influences the bubble departure/lift-off conditions, thus making it necessary to further investigate this effect through a comparison with theoretical models. The bubble growth rate appears to be absolutely insensitive to a change in the mass flux G, thus suggesting that an increase in G only makes the inertia force to rise and, thereby, causes an early departure of the bubble from the nucleation site (Fig. 7b). Meanwhile, the higher the subcooling level is, the more reduced the bubble growth rate appears to be. Probable reasons for this are a strong condensation effect and reduced interface area of the bubble at an increased subcooling temperature. Further research with the use of state-of-the-art visualisation and laser-based techniques might help provide useful insights into the physics of this process towards understanding of the interrelation between the control parameters and the bubble growth process.

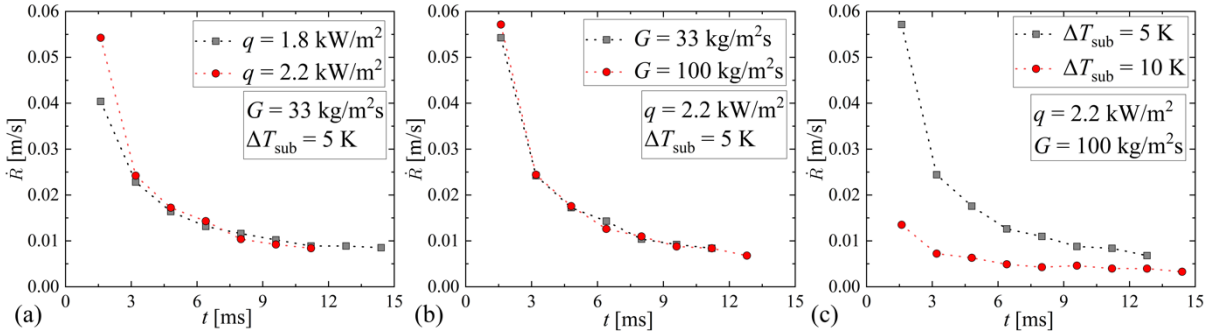


Fig. 7 Bubble growth rate at different: (a) heat fluxes, (b) mass fluxes, and (c) inlet subcooling temperatures.

The bubble sliding velocity V_s also shows a strong dependence on the imposed heat flux and the inlet subcooling level (Fig. 8a and 8c). The mass flux is found to have a minimal effect on V_s like for the bubble growth rate (cf. Figs. 7b and 8b). Velocity fields in the superheated liquid around the bubble might provide useful information about a role of the bulk fluid flow with respect to a transformation of the bubble shape and the resulting motion of the vapour bubble after its lift-off from the wall.

The bubble ebullition frequency $f = 1/t_c$, where t_c is the time difference between consecutive bubble incipiencies from the same nucleation site, over the considered range of the experimental parameters is found to vary from 20 to 90 Hz for HFE-7100 (Fig. 9). A rise in the heat flux results in a higher temperature of the superheated liquid near the heated wall, which facilitates the bubble nucleation and growth, eventually leading to an enhancement in the nucleate boiling heat transfer rate (Fig. 9a). Conversely, an increase of the mass flux makes the convective heat transfer more intense that suppresses

the nucleate boiling, which is seen as a decrease in f (Fig. 9b). A higher inlet subcooling results in a greater temperature gradient in the liquid boundary layer, which leads to an increased convective heat transfer, thus hampering the nucleate boiling and reducing the bubble ebullition frequency (Fig. 9c).

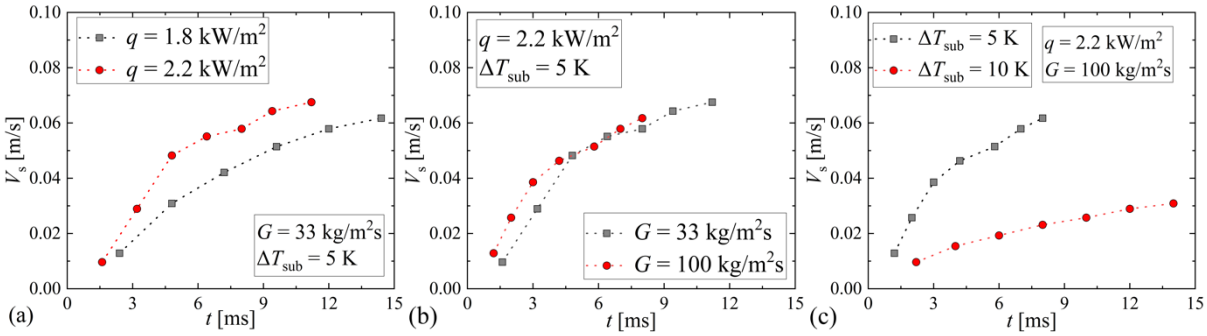


Fig. 8 Bubble sliding velocity at different: (a) heat fluxes, (b) mass fluxes, and (c) inlet subcooling temperatures.

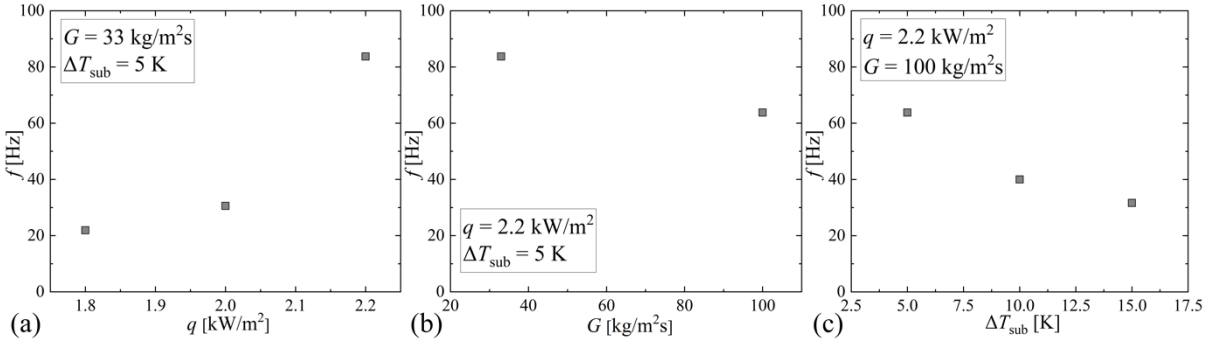


Fig. 9 Variations of the bubble ebullition frequency at different flow conditions.

5. CONCLUSIONS

An experimental investigation of the subcooled flow boiling of HFE-7100 in a vertically oriented square minichannel with a hydraulic diameter of 5 mm was conducted, aiming to study the dependence of the bubble growth rate and sliding velocity of a single vapour bubble on the heat flux, mass flux and inlet subcooling temperature which were varied over the following ranges: 1.8–2.2 kW/m^2, 33–100 kg/m^2·s and 5–15 K, respectively. Sequences of time-lapse images recorded by a high-speed camera were post-processed to extract key bubble size parameters including width, height, base diameter and equivalent diameter, as well as the location of the bubbles geometric centre and upstream/downstream dynamic contact angles. The bubble growth rate and sliding velocity were used to gain insight into the time evolution of the vapour bubble. The bubble dynamic parameters were compared to the isothermal theoretical model by Mikic et al. [7], in order to assess their goodness and to extract information on the change in the superheat level of the liquid surrounding the bubble. Reasonably good agreement of the experimental data with those obtained with the isothermal model of bubble growth was established for the temporal evolution (growth) of the bubble radius. The results further strengthened the hypothesis that bubble growth in refrigerants such as HFE-7100 can be considered as taking place under a close-to-isothermal condition with minimal temperature variations (nearly 0.1 K) in the superheated liquid surrounding the vapour bubble. An effect of the three governing parameters, namely the heat flux, mass flux and inlet subcooling temperature, on the bubble evolution was also explored. It was found that the heat flux and inlet subcooling temperature strongly influence the bubble growth rate and the sliding velocity. In order to gain new insights into the physics of vapour bubble growth and dependence of this process on the imposed experimental conditions, a future study is being currently explored based on the employment of advanced laser-based measurement methods. This forms the scope of future research.

ACKNOWLEDGMENT

This work was supported by the UK Engineering and Physical Sciences Research Council (EPSRC) [grant number EP/T03338X/1], and by the Ministry of Science and Higher Education of the Russian Federation ("Megagrant" project no. 075-15-2019-1888). Data supporting this publication can be obtained on request from cep-lab@imperial.ac.uk. For the purpose of Open Access, the authors have applied a CC BY public copyright licence to any Author Accepted Manuscript version arising from this submission.

NOMENCLATURE

A	Area	[m^2]		**Greek symbols**	
D	Diameter	[m]	ΔT	Temperature difference	[K]
f	Frequency	[Hz]	θ	Dynamic contact angle	[°]
G	Mass flux	[kg/m^2s]			
H	Height	[m]		**Subscripts**	
I	Current	[A]	b	base	
$\dot{m}$	Mass flow rate	[kg/s]	c	cross-section; channel	
P	Pressure; Perimeter	[Pa]; [m]	d	downstream	
q	Heat flux	[W/m^2]	eq	equivalent	
R	Radius	[m]	h	hydraulic; heating	
$\dot{R}$	Growth rate	[m/s]	in	inlet	
T	Temperature	[K]	s	system; sliding	
t	Time	[s]	sat	saturation	
U	Voltage	[V]	sub	subcooled	
V	Volume	[m^3]	sup	superheat	
W	Width	[m]	u	upstream	

REFERENCES

[1] Lin, S., Sefiane, K., Christy, J.R.E., "Prospects of confined flow boiling in thermal management of microsystems," *Appl. Therm. Eng.*, 22(7), pp. 825-837, (2002). **Journal Paper**

[2] Thome, J.R., "Boiling in microchannels: a review of experiment and theory," *Int. J. Heat Fluid Flow*, 25(2), pp. 128-139, (2004). **Journal Paper**

[3] Magnini, M., Pulvirenti, B., Thome, J.R., "Numerical investigation of hydrodynamics and heat transfer of elongated bubbles during flow boiling in a microchannel," *Int. J. Heat Mass Transf.*, 59, pp. 451-471, (2013). **Journal Paper**

[4] Sinha, G.K., Narayan, S., Srivastava, A., "Microlayer dynamics during the growth process of a single vapour bubble under subcooled flow boiling conditions," *J. Fluid Mech.*, 931, (2022). **Journal Paper**

[5] Kossolapov, A., Phillips, B., Bucci, M., "Can LED lights replace lasers for detailed investigations of boiling phenomena?" *Int. J. Multiph. Flow*, 135, p. 103522, (2021). **Journal Paper**

[6] Karayiannis, T.G., Mahmoud, M.M., "Flow boiling in microchannels: Fundamentals and applications," *Appl. Therm. Eng.*, 115, pp. 1372-1397, (2017). **Journal Paper**

[7] Mikic, B.B., Rohsenow, W.M., Griffith, P., "On bubble growth rates," *Int. J. Heat Mass Transf.*, 13(4), pp. 657-666, (1970). **Journal Paper**

[8] Voulgaropoulos, V., Aguiar, G.M., Markides, C.N., Bucci, M., "Simultaneous laser-induced fluorescence, particle image velocimetry and infrared thermography for the investigation of the flow and heat transfer characteristics of nucleating vapour bubbles," *Int. J. Heat Mass Transf.*, 187, p. 122525, (2022). **Journal Paper**

[9] Mukherjee, A., Kandlikar, S.G., Edel, Z.J., "Numerical study of bubble growth and wall heat transfer during flow boiling in a microchannel," *Int. J. Heat Mass Transf.*, 54(15-16), pp. 3702-3718, (2011). **Journal Paper**

[10] Sauvola, J., Pietikäinen, M., "Adaptive document image binarization," *Pattern Recognit.*, 33(2), pp. 225-236, (2000). **Journal Paper**

[11] Moffat, R.J., "Describing the uncertainties in experimental results," *Exp. Therm. Fluid Sci.*, 1(1), pp. 3-17, (1988). **Journal Paper**

[12] Ahmadi, R., Ueno, T., Okawa, T., "Bubble dynamics at boiling incipience in subcooled upward flow boiling," *Int. J. Heat Mass Transf.*, 55(1-3), pp. 488-497, (2012). **Journal Paper**

[13] Ardron, K.H., Giustini, G., Walker, S.P., "Prediction of dynamic contact angles and bubble departure diameters in pool boiling using equilibrium thermodynamics," *Int. J. Heat Mass Transf.*, 114, pp. 1274-1294, (2017). **Journal Paper**